PERGAMON

Computers and Structures 67 (1998) 451–462

Computers & Structures

# CDM based finite element code for concrete in 3-D

Ali H. Al-Gadhib, K. Asad-ur-Rahman, Mohammed H. Baluch *

*Department of Civil Engineering, King Fahd University of Petroleum & Minerals, Dhahran 31261, Saudi Arabia*

Received 8 January 1997; accepted 20 January 1998

**Abstract**

This paper presents a three dimensional finite element code DAMAG3D for nonlinear analysis of concrete type materials modeled as elastic-damage. The CDM model adopted is the one as proposed by SUARIS W, OUYANG C, FERNANDO V. M. Damage model for cyclic loading of concrete. J Engng Mech, American Society of Civil Engineers 1990; 116(5): 1020–35. for monotonic and cyclic loading of concrete structures. Code DAMAG3D is applied to simulate response of concrete under monotonically increasing load paths of uniaxial compression, Brazilian test, strip loading and patch loading, with reasonable correlation established with experimental results and results from other nonlinear constitutive models. 

## 1. Introduction

Continuum damage mechanics (CDM) modeling has given new impetus to the constant search for improvement in constitutive modeling of complex bimodular materials like concrete [1, 2]. With sufficient insight gained into CDM modeling for both brittle & plastic fracture [3, 4], research has been initiated into incorporation of CDM constitutive models into a finite element implementational scheme for solution of problems of engineering interest [5–7]. Chow and Wang in refs [5, 6] have considered finite element formulation of CDM models simulating ductile fracture, with Ghrib and Tinawi [7] focussing on the evergreen problem of concrete gravity dams.

This paper is a 3-D finite element formulation for a concrete like material whose behavior is simulated by the CDM model as presented by Suaris, Ouyang and Fernando [3]. The model assumes behavior of concrete to be elastic-damage, with plastic behavior ignored. The model has several positive features, including (i) the ability to accumulate damage leading to failure under cyclic loading; (ii) incorporation of influence of stress induced anisotropy by consideration of damage as a vector; (iii) use of strain energy release rate space for description of damage evolution (in contrast to stress space); and (iv) simplicity of form without recourse to an exorbitantly large number of calibration constants.

## 2. Elastic potential $\Lambda$

An elastic complementary free energy potential function $\Lambda$ is assumed in the form

$$\Lambda = \Lambda(\boldsymbol{\sigma}_{ij}, \boldsymbol{\omega}_i), \tag{1}$$

where $\boldsymbol{\sigma}_{ij}$ = stress tensor and $\boldsymbol{\omega}_i$ the damage vector in a principal framework. The incremental quantity $\rho d\Lambda$ ($\rho$ = mass density) is then given by

$$\rho d\Lambda = \rho \frac{\partial \Lambda}{\partial \boldsymbol{\sigma}_{ij}} d\, bf \sigma_{ij} + \rho \frac{\partial \Lambda}{\partial \boldsymbol{\omega}_i} d\sigma_i, \tag{2}$$

which yields the constitutive relations in terms of conjugate variables $\epsilon_{ij}$ and $R_i$ as

$$\epsilon_{ij} = \rho \frac{\partial \Lambda}{\partial \boldsymbol{\sigma}_{ij}} \tag{3a}$$

$$R_i = \rho \frac{\partial \Lambda}{\partial \boldsymbol{\omega}_i}, \tag{3b}$$

where $\epsilon_{ij}$ is the classical strain tensor and $R_i$ is interpreted as the strain energy release rate associated with

* Author to whom correspondence should be addressed.

0045-7949/98/$19.00 
PII: S0045-7949(98)00044-3

the damage process. The components of the strain energy release rate vector are generally referred to as the force conjugates of the damage components.

The use of the Clausius–Duhem inequality in terms of the complementary free energy function leads to the condition

$$R_i \dot{\omega}_i > 0. \quad (4)$$

## 3. Bounding surface damage model

In order to construct a rational model accounting for damage growth, concepts are borrowed from incremental theory of plasticity in general and the bounding surface plasticity model in particular as introduced by Dafalias and Popov [8]. The Dafalias–Popov plasticity bounding surface model requires definition of multiple surfaces in stress space. However, the fundamental surfaces of the Suaris model are best described in a strain energy release space:

$$f = (R_i R_i)^{1/2} - R_c/b = 0 \quad (5)$$

$$F = (\bar{R}_i \bar{R}_i)^{1/2} - R_c = 0 \quad (6)$$

$$f_o = (R_i R_i)^{1/2} - 0.08 = 0 \quad (7)$$

Here, $f$ is the loading function surface, $F$ is the bounding surface, $f_o$ is a limit fracture surface (Fig. 1), $\bar{R}_i$ an image point on $F = 0$ associated with a given point $R_i$ on $f = 0$ defined by a mapping rule

$$\bar{R}_i = bR_i \quad (8)$$

$$b = R_c/(R_i R_i)^{1/2} \quad (9)$$

with the mapping parameter $b$ ranging from an initial value of $\infty$ to a limiting value of 1 on growth of loading surface to coalesce with bounding surface. $R_c$ is a parameter of the model, and can be calibrated to the standard uniaxial compression test. Suaris has suggested the use of $R_c = 0.63$, but obviously this parameter should vary as the concrete compressive strength $f'_c$ varies.

Damage is hypothesized to accumulate at levels of strain energy release rate resulting in the loading surface '$f$' traversing the limit fracture surface '$f_o$', and rupture in the damage sense is said to occur when the '$f$' surface grows large enough to coalesce with the bounding surface $F$ fixed in the $R_i$ space.

## 4. Damage incremental stress-strain law

Consider the decomposition of the stress and strain tensor into their principal values (i.e. positive and

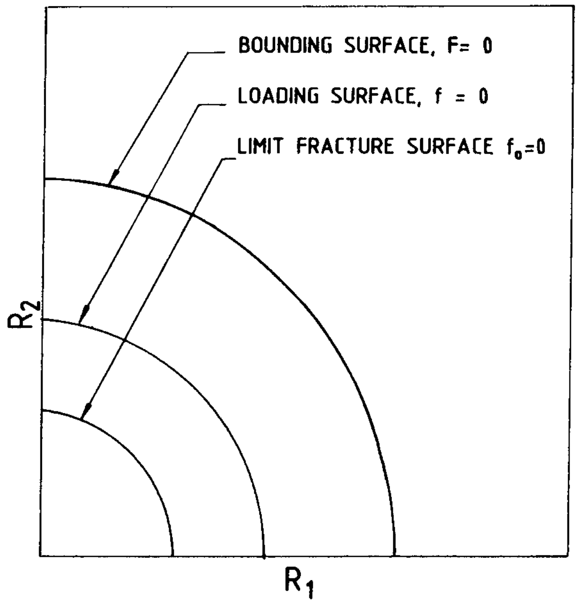


Fig. 1. Illustration of bounding, loading & limit fracture surfaces in 2-D.

negative eigenvalues) given by

$$\underline{\sigma} = \underline{\sigma}^+ + \underline{\sigma}^- \quad \text{and} \quad \underline{\epsilon} = \underline{\epsilon}^+ + \underline{\epsilon}^- \quad (10)$$

The complementary free-energy function $\rho\Lambda$ and the strain energy function $\rho\psi$ may be written as

$$\rho\Lambda = \frac{1}{2}(\underline{\sigma}^+ \mathbf{C}_I \underline{\sigma}^+ + \underline{\sigma}^- \mathbf{C}_{II} \underline{\sigma}^-) \quad (11)$$

$$\rho\psi = \frac{1}{2}(\underline{\epsilon}^+ \mathbf{D}_I \underline{\epsilon}^+ + \underline{\epsilon}^- \mathbf{D}_{II} \underline{\epsilon}^-) \quad (12)$$

where $\mathbf{C}_\mathrm{I}$ and $\mathbf{C}_\mathrm{II}$ are the compliance matrices for tensile and compressive stresses, respectively, and $\mathbf{D}_\mathrm{I}$ and $\mathbf{D}_\mathrm{II}$ are their respective inverses such that:

$$\mathbf{D}_I = [\mathbf{C}_I]^{-1} \quad \text{and} \quad \mathbf{D}_{II} = [\mathbf{C}_{II}]^{-1} \quad (13)$$

Expressions for $\mathbf{D}_\mathrm{I}$ and $\mathbf{D}_\mathrm{II}$ are included in the Appendix.

The decomposition of the elastic potential into tensile and compressive components enables the modeling of the different crack mechanism in tension and compression. The compliance matrices as proposed in ref. [3] may be written as

$$\mathbf{C}_I = \frac{1}{E_o}\begin{bmatrix} \frac{1}{(1-\alpha\omega_1)} & -\nu & -\nu \\ -\nu & \frac{1}{(1-\alpha\omega_2)} & -\nu \\ -\nu & -\nu & \frac{1}{(1-\alpha\omega_3)} \end{bmatrix} \quad (14)$$

$$\mathbf{C}_{II} = \frac{1}{E_o}\begin{bmatrix} \frac{1}{(1-\beta\omega_2)(1-\beta\omega_3)} & \frac{-\nu}{(1-\omega_1)(1-\omega_2)} & \frac{-\nu}{(1-\omega_1)(1-\omega_3)} \\ \frac{-\nu}{(1-\omega_1)(1-\omega_2)} & \frac{1}{(1-\beta\omega_1)(1-\beta\omega_3)} & \frac{-\nu}{(1-\omega_2)(1-\omega_3)} \\ \frac{-\nu}{(1-\omega_1)(1-\omega_3)} & \frac{-\nu}{(1-\omega_2)(1-\omega_3)} & \frac{1}{(1-\beta\omega_1)(1-\beta\omega_2)} \end{bmatrix} \quad (15)$$

where $E_o$ = modulus of elasticity and $\nu$ = the Poisson's ratio of the uncracked concrete; and $\boldsymbol{\omega}_1$, $\omega_2$, $\omega_3$ are the components of damage in the three principal directions. The form of compliance matrix $\mathbf{C}_I$ is based on the assumption that crack growth in a particular plane increases the flexibility of the material along an axis perpendicular to it but has no influence on the in-plane flexibility. The parameters $\alpha$ and $\beta$ are introduced to account for influence of stress intensity factors and the tortuosity (or cross-effect) of cracks, respectively.

From the strain energy function of Eq. (12), one may find the constitutive relations in total and incremental form as

$$\boldsymbol{\sigma}_i = \rho\frac{\partial\psi}{\partial\boldsymbol{\epsilon}_i}(\boldsymbol{\epsilon}_i, \mathbf{D}_{kl}(\boldsymbol{\omega}_n)) = \mathbf{D}^I_{ij}\boldsymbol{\epsilon}^+_j + \mathbf{D}^{II}_{ij}\boldsymbol{\epsilon}^-_j, \quad (16)$$

$$d\boldsymbol{\sigma}_i = \mathbf{D}^I_{ij}d\boldsymbol{\epsilon}^+_j + \mathbf{D}^{II}_{ij}d\boldsymbol{\epsilon}^-_j + \mathbf{D}^I_{ij}\boldsymbol{\epsilon}^+_j + d\mathbf{D}^{II}_{ij}\boldsymbol{\epsilon}^-_j. \quad (17)$$

In finite element methods, usually the primary unknowns are the displacement or incremental displacement and the current strains and incremental strains can be determined subsequently. However, to calculate increment of stress from Eq. (17), one needs the damage evolution equations for computation of $\mathbf{D}_I$, $\mathbf{D}_{II}$, $d\mathbf{D}_I$ and $d\mathbf{D}_{II}$.

## 5. Damage evolution equations

The damage growth rate is hypothesized to be conceptually similar to increments of plastic strain as in associative theory of plasticity. Using the normality condition, increment of damage is expressed as

$$d\boldsymbol{\omega}_i = dL\frac{\partial f}{\partial R_i} \quad (18)$$

where $dL$ is a loading index chosen to satisfy $R_i\boldsymbol{\omega}_i > 0$ (in a manner similar to $\sigma_{ij}d\epsilon^I_{ij} > 0$). This yields

$$dL = \frac{df}{H} = \frac{1}{H}\frac{\partial f}{\partial R_j}dR_j > 0 \quad \text{(loading)} \quad (19a)$$

$$dL = 0 \quad \text{(unloading)} \quad (19b)$$

and $H$ = damage modulus. Reducing (19a) to a uniaxial test, the damage modulus $H = dR/d\boldsymbol{\omega}$ can be calibrated similar to the calibration of the plastic modulus as introduced by Dafalias and Popov [8] in the bounding surface theory of plasticity. Suaris, Ouyang and Fernando [3] used a regressed hyperbolic form for the damage modulus

$$H = H(\delta) = \mathbf{D}\frac{\delta}{<\delta_{in} - \delta>} \quad (20)$$

where $\mathbf{D}$ = 2.65, $\delta_{in}$ = initial distance between the limit fracture surface and the bounding surface and $\delta$ = distance between the loading and bounding surface = $1 - 1/b$ (Fig. 2).

With the assumed form of $f$ as given by Eq. (5), $\partial f/\partial R_i = R_i/(R_jR_j)^{1/2}$ and $dL = R_jdR_j/[H(R_kR_k)^{1/2}]$. Thus, increment of the damage vector requires knowledge of increments of strain energy release rate ($dR_i$) and current strain energy release rate vector $R_i$. Using the elastic complementary free-energy function $\Lambda$ and $R_k$ relationship, one obtains

$$R_k(\sigma, \boldsymbol{\omega}_i) = \rho\frac{\partial\Lambda}{\partial\boldsymbol{\omega}_k} = \frac{1}{2}\left[\left(\sigma^+_i\frac{\partial C^I_{ij}}{\partial\boldsymbol{\omega}_k}\sigma^+_j\right) + \left(\sigma^-_i\frac{\partial C^{II}_{ij}}{\partial\boldsymbol{\omega}_k}\sigma^-_j\right)\right] \quad (21)$$

$$\begin{aligned} dR_k = &\left(\sigma^+_i\frac{\partial C^I_{ij}}{\partial\boldsymbol{\omega}_k}d\sigma^+_j + \sigma^-_i\frac{\partial C^{II}_{ij}}{\partial\boldsymbol{\omega}_k}d\sigma^-_j\right) \\ &+\frac{1}{2}\left(\sigma^+_i\frac{\partial}{\partial\boldsymbol{\omega}_l}\left[\frac{\partial\mathbf{C}^I_{ij}}{\partial\boldsymbol{\omega}_k}\right]d\boldsymbol{\omega}_l\sigma^+_j \right.\\ &\left.+\sigma^-_i\frac{\partial}{\partial\boldsymbol{\omega}_l}\left[\frac{\partial\mathbf{C}^{II}_{ij}}{\partial\boldsymbol{\omega}_k}\right]d\boldsymbol{\omega}_l\sigma^-_j\right) \end{aligned} \quad (22)$$

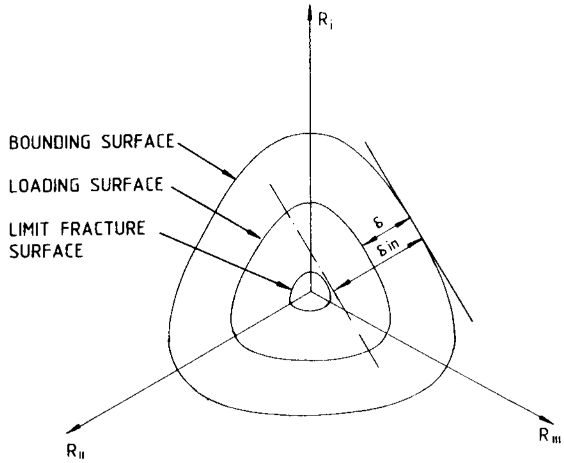


Fig. 2. Schematic of normalized distance $\delta$ in R-deviatoric plane.

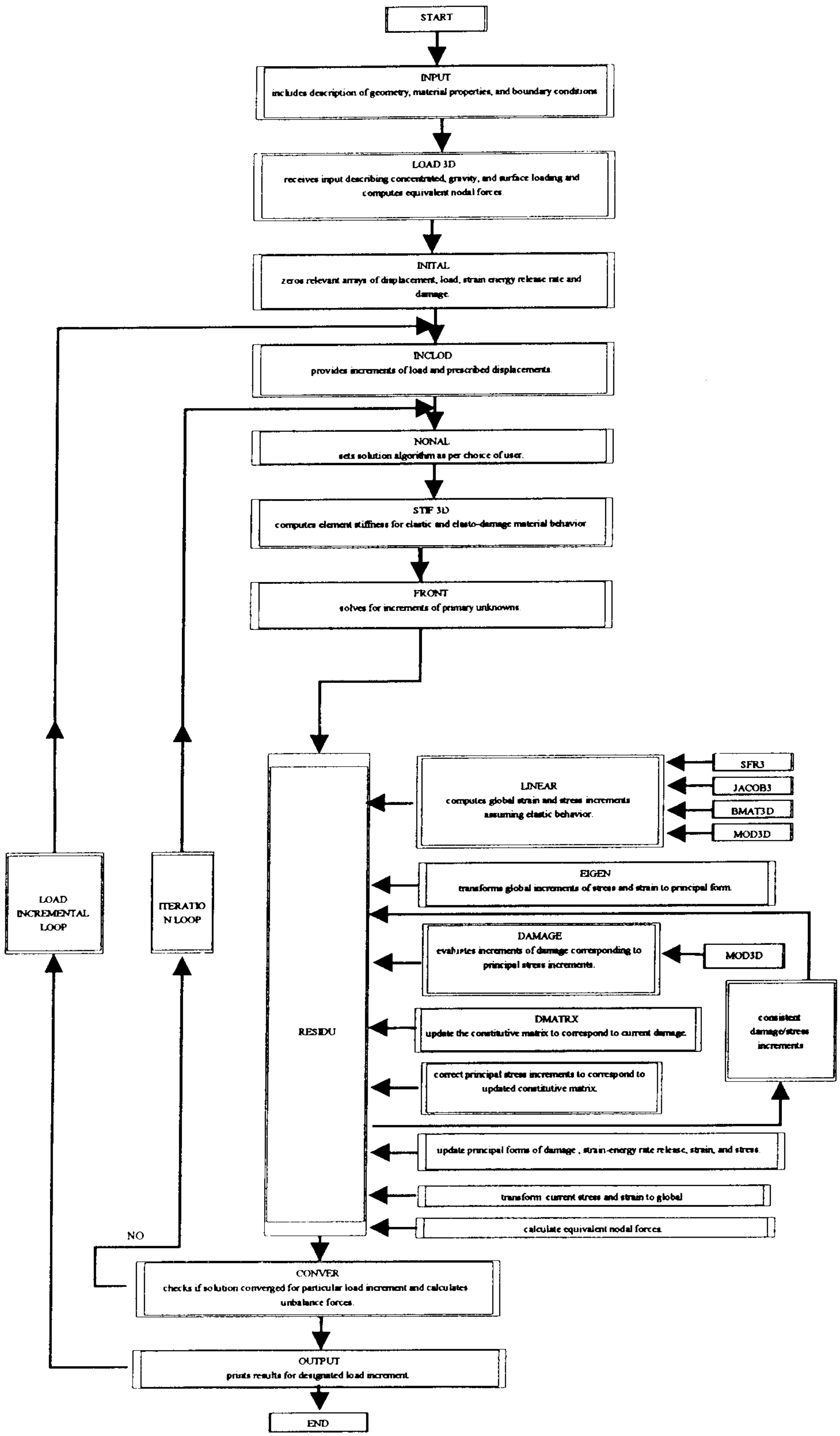


Fig. 3. Flow chart of DAMAG3D.

## 6. Alternate representation of damage growth

In order to observe the model's ability to predict strain softening, it is essential to recast the increment in damage, $d\boldsymbol{\omega}_i$, in an alternate form. Khan *et al.* [9], in a recent contribution have shown that for a strain control test,

$$dL = \frac{\frac{\partial f}{\partial R_k}\frac{\partial R_k}{\partial \boldsymbol{\varepsilon}_j} d\boldsymbol{\varepsilon}_j}{H - \frac{\partial f}{\partial R_k}\frac{\partial R_k}{\partial \boldsymbol{\omega}_l}\frac{\partial f}{\partial R_l}} \tag{23}$$

where $d\boldsymbol{\omega}_i$ is as given by Eq. (18).

The phenomenon of strain softening is demonstrated for the case of uniaxial compression. For the Suaris model,

$$\rho\Lambda = \frac{\sigma^2}{2E_0(1-\beta\boldsymbol{\omega}_2)(1-\beta\boldsymbol{\omega}_3)} \tag{24}$$

with

$$R_2' = R_2(\sigma, \boldsymbol{\omega}) = \frac{\beta\sigma^2}{2E_0(1-\beta\boldsymbol{\omega}_2)^2(1-\beta\boldsymbol{\omega}_3)} \tag{25a}$$

$$R_3 = R_3(\sigma, \boldsymbol{\omega}) = \frac{\beta\sigma^2}{2E_0(1-\beta\boldsymbol{\omega}_2)(1-\beta\boldsymbol{\omega}_3)^2}, \tag{25b}$$

where due to symmetry $\boldsymbol{\omega}_2 = \boldsymbol{\omega}_3 = \boldsymbol{\omega}$ and $\boldsymbol{\omega}_1 = 0$.

The loaded direction corresponds to the 1-coordinate. The total stress–strain relation is given by

$$\sigma = E_0\boldsymbol{\varepsilon}_1(1-\beta\boldsymbol{\omega}_2)(1-\beta\boldsymbol{\omega}_3) \tag{26}$$

Using Eq. (26) in (25),

$$R_2 = \frac{\beta\boldsymbol{\varepsilon}_1^2 E_0(1-\beta\boldsymbol{\omega}_3)}{2} \tag{27a}$$

$$R_3 = \frac{\beta\boldsymbol{\varepsilon}_1^2 E_0(1-\beta\boldsymbol{\omega}_2)}{2} \tag{27b}$$

From Eq. (5)

$$\left[\frac{\partial f}{\partial R_i}\right] = \left[0 \ \ \frac{1}{\sqrt{2}} \ \ \frac{1}{\sqrt{2}}\right] \tag{28}$$

and from Eq. (27)

$$\left[\frac{\partial R_1}{\partial \boldsymbol{\omega}_i}\right] = [0 \ 0 \ 0] \tag{29a}$$

$$\left[\frac{\partial R_2}{\partial \boldsymbol{\omega}_i}\right] = \left[0 \ 0 \ -\frac{\beta^2\boldsymbol{\varepsilon}_1^2 E_0}{2}\right] \tag{29b}$$

$$\left[\frac{\partial R_3}{\partial \boldsymbol{\omega}_i}\right] = \left[0 \ -\frac{\beta^2\boldsymbol{\varepsilon}_1^2 E_0}{2} \ 0\right] \tag{29c}$$

$$\left[\frac{\partial R_1}{\partial \boldsymbol{\varepsilon}_i}\right] = [0 \ 0 \ 0] \tag{29d}$$

$$\left[\frac{\partial R_2}{\partial \boldsymbol{\varepsilon}_i}\right] = [\beta\boldsymbol{\varepsilon}_1 E_0(1-\beta\boldsymbol{\omega}) \ 0 \ 0] = \left[\frac{\partial R_3}{\partial \boldsymbol{\varepsilon}_i}\right] \tag{29e}$$

Carrying out the appropriate matrix multiplications as defined in Eq. (23) results in

$$dL = \frac{\sqrt{2}\beta\boldsymbol{\varepsilon}_1 E_0(1-\beta\boldsymbol{\omega})}{\left(H + \frac{\beta^2\boldsymbol{\varepsilon}_1^2 E_0}{2}\right)} d\boldsymbol{\varepsilon}_1 \tag{30}$$

Ref. [9] also delineates the form of incremental stress strain law as

$$d\sigma_i = \mathbf{D}_{im}^{ed} d\boldsymbol{\varepsilon}_m \tag{31}$$

where $\mathbf{D}_{im}^{ed}$ is the elasto-damage tangential stiffness given by

$$\mathbf{D}_{im}^{ed} = \mathbf{D}_{im} + \boldsymbol{\varepsilon}_n \frac{\partial D_{in}}{\partial \boldsymbol{\omega}_q}\frac{\partial f}{\partial R_q}\frac{\frac{\partial f}{\partial R_k}\frac{\partial R_k}{\partial \boldsymbol{\varepsilon}_m}}{H - \frac{\partial f}{\partial R_l}\frac{\partial R_l}{\partial \boldsymbol{\omega}_l}\frac{\partial f}{\partial R_l}} \tag{32}$$

where $\mathbf{D}_{im}$ matrix is detailed in the Appendix.

For the case of uniaxial compression, the only essential term of the $\mathbf{D}_{im}$ matrix is

$$\mathbf{D}_1 = E_0(1-\beta\boldsymbol{\omega}_2)(1-\beta\boldsymbol{\omega}_3) \tag{33}$$

with

$$\left[\frac{\partial D_1}{\partial \boldsymbol{\omega}_i}\right] = \beta E_0[0 - (1-\beta\boldsymbol{\omega}) - (1-\beta\boldsymbol{\omega})] \tag{34}$$

substitution of Eqs. (33) and (34) into Eq. (31) leads to the incremental $\sigma - \varepsilon$ law

$$d\sigma = \left(E_0(1-\beta\boldsymbol{\omega})^2 - \frac{2\beta^2\boldsymbol{\varepsilon}_1^2 E_0(1-\beta\boldsymbol{\omega})^2}{H + \frac{\beta^2\boldsymbol{\varepsilon}_1^2 E_0}{2}}\right) d\boldsymbol{\varepsilon}_1 \tag{35}$$

## 7. Program DAMAG3D

A computer code DAMAG3D has been developed for the elasto-damage analysis of three dimensional structures using a twenty noded serendipity isoparametric element. Three degrees of freedom are specified at each node, corresponding to three displacements at that node. Stresses, strains and change in the characteristics of the material are monitored at Gauss integration points within each element. Any Gauss point may remain elastic or undergo damage or fail. Normal integration scheme is employed using $3 \times 3 \times 3$ integration rule.

The program is written in a FORTRAN code, and is expressed in a modular form consisting of various subroutines called from the main program and from within themselves. It has been written along the format of two-dimensional elasticity and plasticity programs, ELAS2D & PLAS2D, as developed by Profs Hinton and Owen in their classical texts on finite element modelling [10, 11], with extensions made to three-dimensional analysis wherever deemed appropriate.

The major subroutines and their functions are outlined in the flow chart shown in Fig. 3. In addition to incorporation of three-dimensional features in subroutines such as LOAD3D and INPUT, the two subroutines RESIDU and STIF3D reflect the most significant changes by virtue of incorporation of a new material model.

Subroutine RESIDU essentially corrects the stresses at each Gauss point to correspond to the updated constitution of the material. It then proceeds to establish the unbalance of forces in each element resulting from the correction of stresses at each Gauss point. This unbalance is the difference in the consistent load vector (expressed in terms of external forces) and the equivalent nodal forces (expressed in terms of internal stresses). This unbalance is reduced in successive iterations to a tolerable value in order to meet the desired degree of convergence which is ensured in subroutine CONVER.

Subroutine LINEAR passes to RESIDU linearized increments of stress and strain assuming elastic behavior. Subroutine EIGEN (called from RESIDU) then transforms the global stress and strain increments to principal form, ordering and separating tension and compression components. Subroutines DAMAGE and DMATRX (both called from RESIDU) are used as components in an internal iterative loop to evaluate increment in damage and update the constitutive matrix in order to correct the increments of stress in a principal framework. This internal iterative loop is terminated on attaining increments of damage and strain energy release consistent with increments of stress. After updating of total stress and strain tensors in principal framework, the stress tensor is then transformed to a global framework for use in evaluation of equivalent nodal forces prior to computation of residual or unbalanced forces for each element.

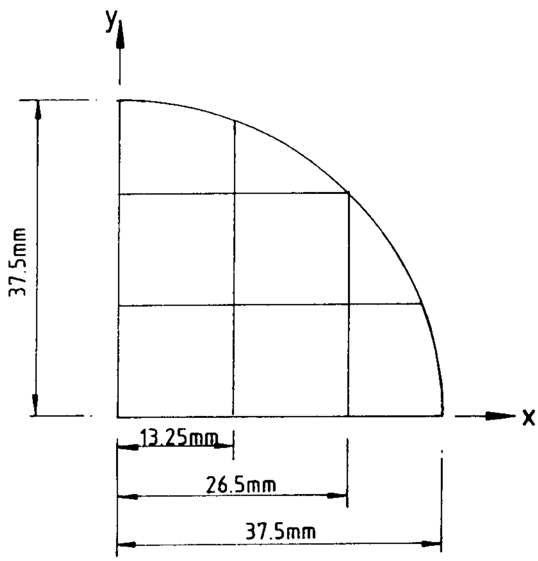


Fig. 4. Plan view of one quarter of concrete cylinder.

## 8. Finite element predictions and example verifications

In order to verify the predictions based on the CDM model of ref. [3], four problems are selected for which experimental results and/or predictions corresponding to alternative models are available for comparison. The problems selected include uniaxial compression test, Brazilian test, concentric strip, and patch loading of rectangular prism. Results are presented in terms of ultimate load, stress strain response curves and damage topography in terms of damage contours.

Calibration parameters α and β were taken as 4 and 0.1 as recommended in ref. [3]. All parameters of the model ($R_c$, **D**, α, β) are unit biased, i.e. they are to be used in conjunction with the inch pound system. Results however are presented in the metric unit system.

### *8.1. Example 1: Uniaxial compression test*

A standard concrete cylinder of diameter 75 mm and of height 100 mm is subjected to uniaxial compression. Utilizing triaxial symmetry, one eighth of the cylinder is used and discretized into eight isoparametric elements (Fig. 4), each of which contained 27 sampling points (Gauss points or integration points) according to which a total of $27 \times 8 = 216$ sampling points are contained within the part under consideration. The compressive strength, modulus of elasticity and Poisson's ratio were taken as 38.6 MPa, 32.4 GPa and 0.19, respectively. The boundary conditions are incorporated to reflect three planes of symmetry on which the nodal displacement perpendicular to the plane of symmetry is restrained and only the tangential displacements are allowed. Moreover, nodes located along the line of intersection of the two vertical planes of symmetry are allowed to move freely only along the line of intersection.

Although here the compression test is treated as a 3-D problem, it is essentially a 1-D problem where all the Gauss points experience uniform displacement, stress and strain. The load $P$ has been applied incrementally in terms of uniform stress $\sigma$ such that $P = \sigma A$, where $A$ is the area of the cross section. It has been found that $P_{ult} = 167$ kN compared to the corresponding experimental value of 176 kN. Due to symmetry, only one independent component of damage $\omega_2 = \omega_3 = \omega$ is non-zero and which is a monotonically increasing function of the applied stress during loading. The plot of damage vs normalized applied stress is shown in Fig. 5.

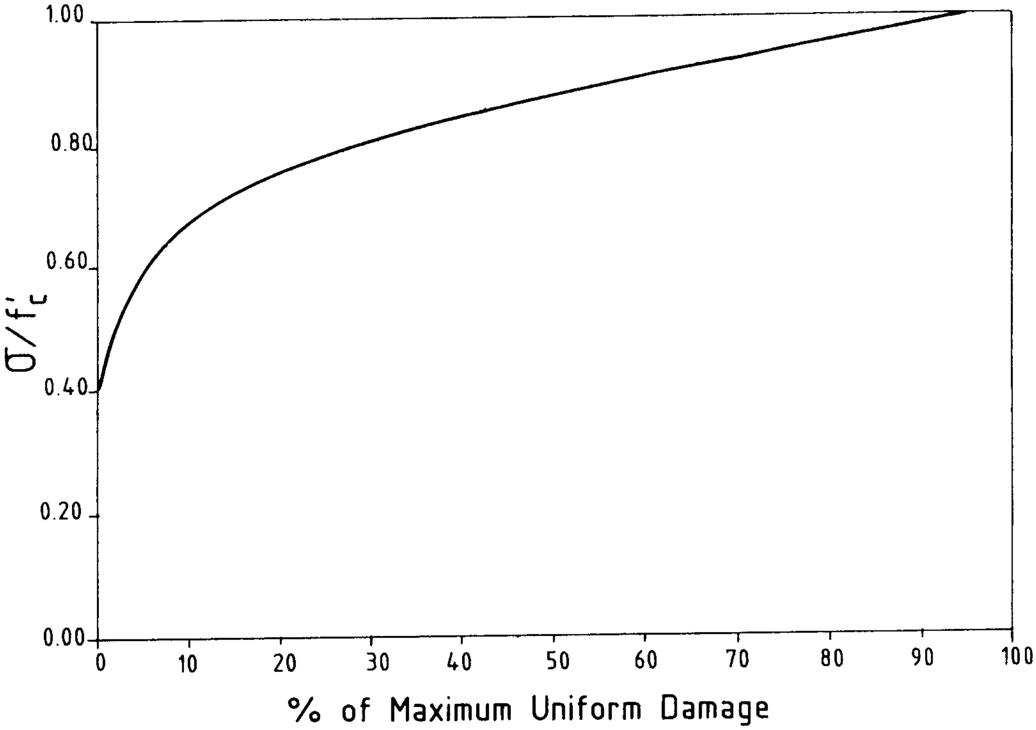


Fig. 5. Damage at different load levels.

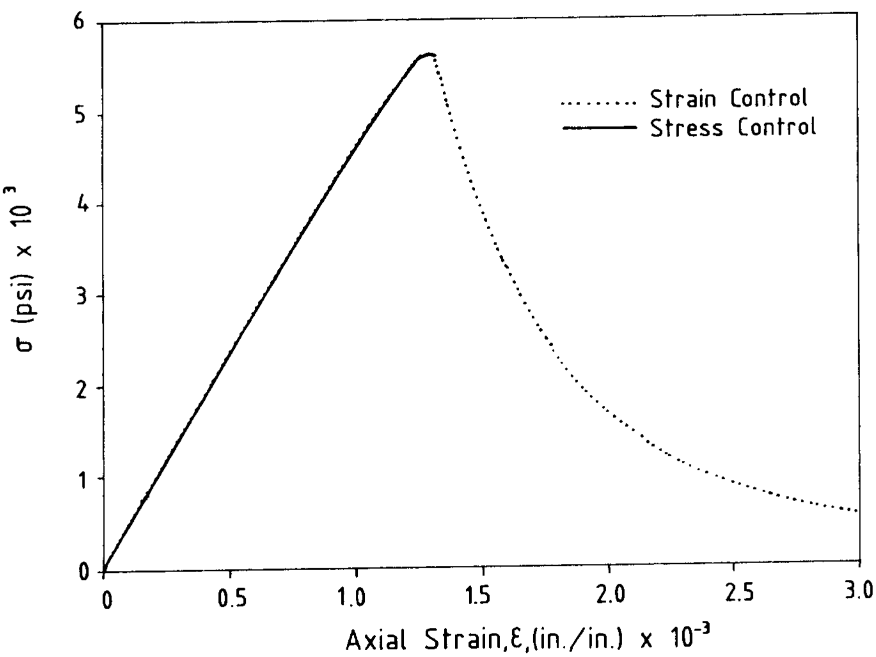


Fig. 6. Stress-strain curves for uniaxial compression.

Fig. 6 shows the ability of the alternate formulation approach to model the phenomenon of strain softening. Results for both strain control and stress control are echoed, with the strain softening segment being sensitive to the form of damage modulus $H$ chosen i.e. the magnitude of **D** in Eq. (20). A form of $D$ can be chosen to vary with the concrete compressive strength $f'_c$. This variation may be calibrated to obtain the best fit to experimental results of post-peak softening for normal and high strength concretes.

### 8.2. Example 2: Brazilian test

A concrete cylinder of length 300 mm with diameter **D** = 150 mm is placed with its axis horizontal and subjected to a line load spread over a width of **D**/8 to simulate the loading conditions of the Brazilian test, see Fig. 7. Material properties are specified as: compressive strength $f'_c = 32$ MPa, modulus of elasticity $E$ = 32.4 GPa, and Poisson's ratio $\nu$ = 0.2. The Brazilian test has been analyzed numerically by Resende [12] as a two-dimensional plane strain problem using a 2-D CDM model. Due to symmetry, only one eighth of the cylinder is investigated and discretized into 27 isoparametric elements, each of which contained 27 sampling points to yield a total of 27 × 27 sampling points where stresses and strains are monitored.

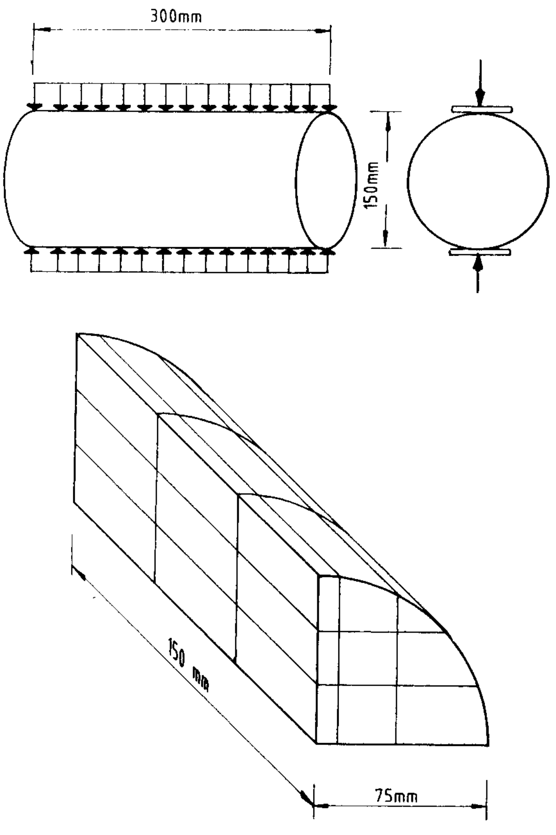


Fig. 7. Finite element mesh of cylinder for Brazilian test.

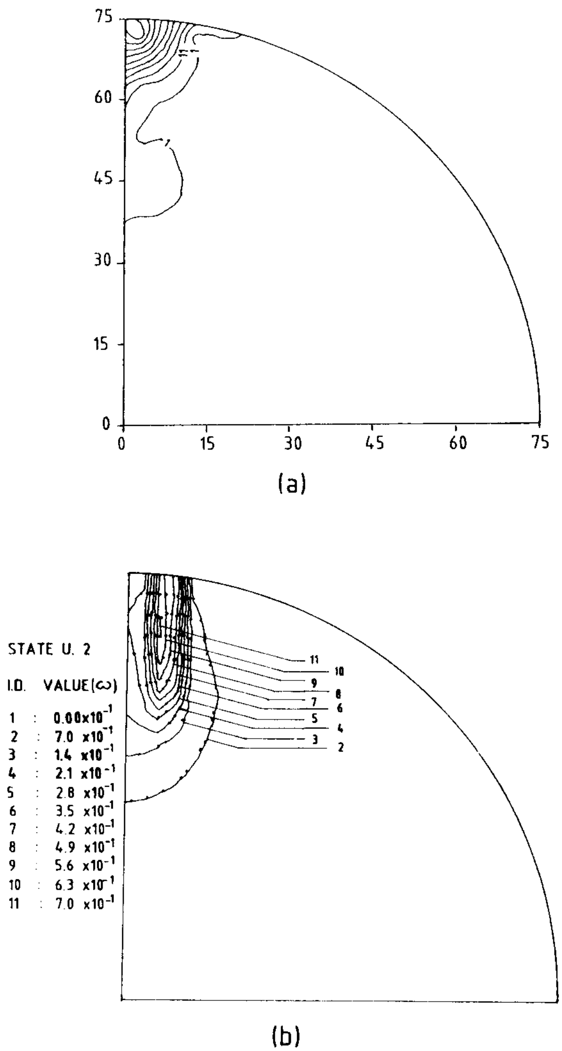


Fig. 8. (a) Damage distribution based on CDM model of ref. [3]. (b) Damage distribution based on CDM model of ref. [12].

The load has been applied incrementally until failure occurs. The value of the total accumulated load at which the last increment is converged is referred to as the failure load. For the Brazilian test, the failure or ultimate load $P_{ult} = 235$ kN as compared to $P_{ult} = 181$ kN of Resende [11]. The damage contour patterns are shown in Fig. 8 and as anticipated, the maximum damage occurs just beneath the applied load and diminishing rapidly toward the center. Fig. 8 reveals that although the extent of damaged zone is almost the same for both Resende [12] and predictions based on

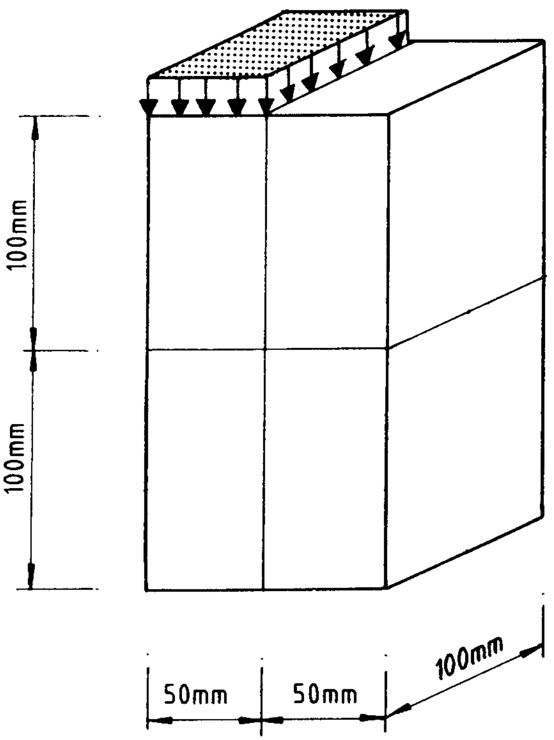


Fig. 9. Finite element mesh for concrete prism.

ref. [3] which is localized into the upper left region, the damage contour pattern corresponding to Suaris damage model is showing symmetry about the centerline which is in contrast to that exhibited by Resende's model.

The Brazilian test is often used to predict the direct tensile strength of concrete as given by $f'_t = 2P_{ult}/\pi LD$, where $L$ and $D$ are the length and diameter of the cylinder, respectively. Based on the results obtained here, the tensile strength $f'_t$ is calculated to be 3.32 MPa which is nearly 0.1 $f'_c$. This value affirms the maintenance of the ratio $f'_t/f'_c$ for the Brazilian test stress path as a consequence of the parameter $\alpha$ calibrated using the stress path described in a direct tension test.

### 8.3. Example 3: Strip Loading on a rectangular prism

A concrete rectangular prism of square cross section 200 mm × 200 mm and of height 400 mm is subjected to a strip loading of width 100 mm as shown in Fig. 9. Due to symmetry in geometry and loading conditions, one eighth of the prism is considered to model the problem together with the appropriate boundary conditions along planes of symmetry. Consequently, the part under consideration is of dimensions 100 mm × 100 mm × 200 mm which has been discretized into four elements, each of which contained 27 sampling points. Accordingly, 27 × 4 = 108 sampling points are available to describe the stress and strain distribution within the body. Uniaxial compressive strength concrete $f'_c$ is taken as 38.6 MPa with modulus of elasticity $E$ = 32.4 GPa. To maintain symmetry, displacements perpendicular to the plane of symmetry are restrained. After incrementing the uniform applied load, the ultimate load was found to be 557 kN as compared to the predictions of Gonzalez *et al.* [13], who solved the same problem based on a 3-D plasticity model and found the load to be 562 kN. In both models the predicted ultimate loads are little bit overestimated as compared to the experimental value of 515 kN. The damage distribution on the plane and across the depth is shown in Fig. 10 where damage is noted to occur only in quarter zones adjacent to the top and bottom of the specimen. Also, it is noticed that damage (in plan) is maximum toward the center and decreases as one moves away.

### 8.4. Example 4: Patch Loading on a rectangular prism

A concrete rectangular prism of dimensions similar to the one used in Example 3 is subjected to a concentric patch loading as shown in Fig. 11. Utilizing symmetry of geometry and loading conditions, one fourth of the prism is considered to model the problem together with the appropriate boundary conditions along planes of symmetry. The part under consideration is of dimension 100 mm × 100 mm × 400 mm, discretized into eight elements, each of which contained 27 Gauss sampling points. Accordingly, 27 × 8 = 216 sampling points are available to describe the stress and strain distribution within the body. Material properties are specified as: compressive strength $f'_c = 28.8$ MPa, modulus of elasticity $E$ = 25.4 GPa and Poisson's ratio $\nu$ = 0.17. To maintain symmetry, displacements perpendicular to the plane of symmetry are restrained. Behavior of the prism is studied using stress-controlled conditions by applying a patch load of uniform intensity throughout the loaded area.

Sampling points at the top and bottom of the prism exhibit a triaxial compressive state of stress with dominant components being in the loaded direction towards the center of the prism. These stresses tend to reduce as one moves away in the horizontal and vertical directions. In other layers of sampling points, compression–tension–tension states of stress are observed. It is this combined tension–compression state that leads to accelerated damage, resulting in average compressive stresses at ultimate load of lower magnitude than in the case of uniformly compressed prisms. The ultimate load was found to be 359 kN as compared to 323 kN predicted by Gonzalez *et al.* using an elasto-plastic

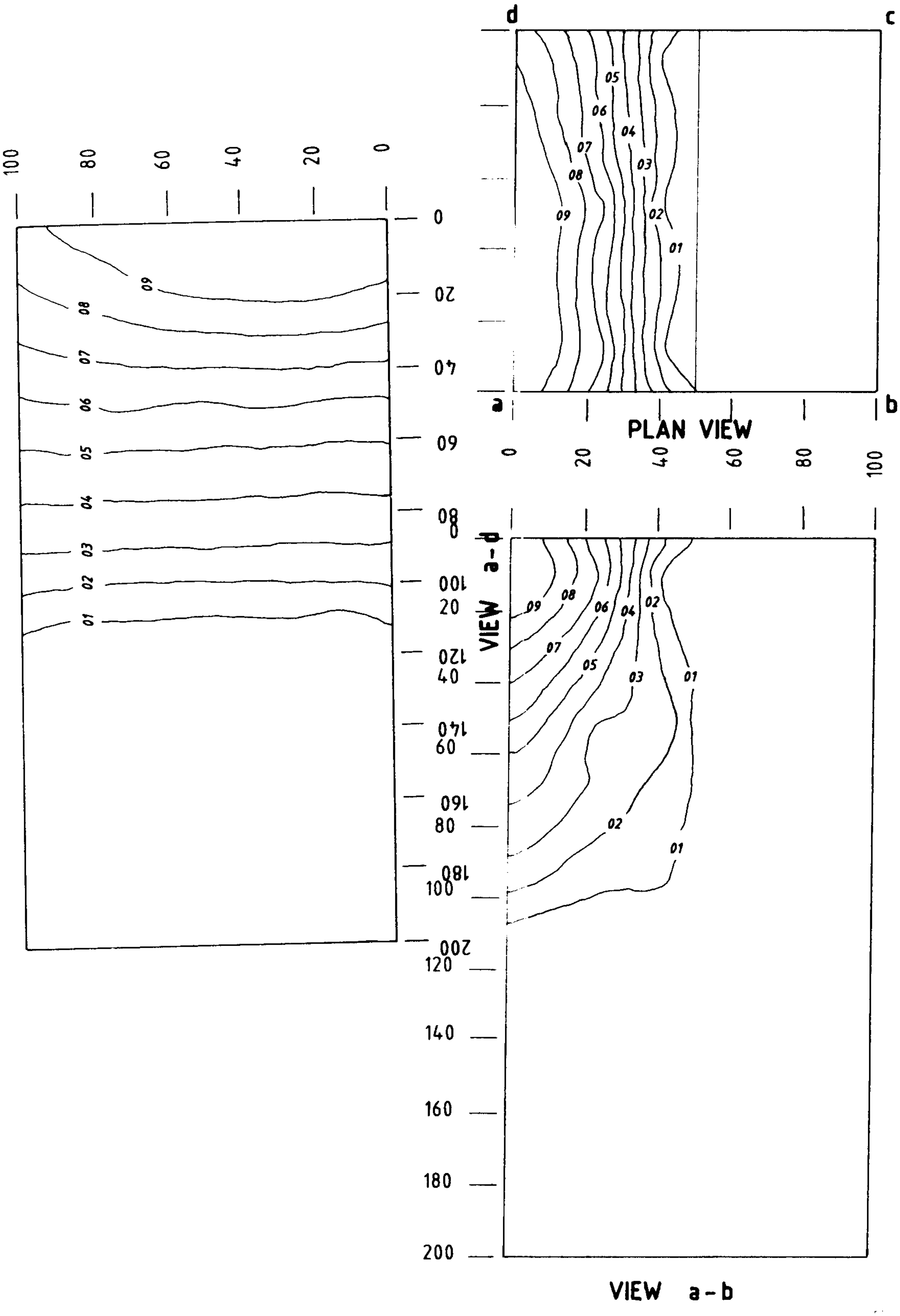


Fig. 10. Damage distribution in prism under strip loading.

model [13] and 314 kN by Niyogi [14] obtained experimentally. Damage is initiated at about fifty percent of the failure load.

## 9. Conclusions

A computer code DAMAG3D has been written to model behavior of concrete under monotonically increasing loading, using a CDM model as presented by Suaris *et al.* [3], where concrete is treated as a bimodular degraded material. The finite element code is developed using the format standardized by Profs. Hinton and Owen in their classical treatment of problems of elasticity, elasto-plasticity and viscoplasticity. In contrast to elasto-plasticity, the software coding for an elasto-damage media requires introduction of an extra internal iterative loop in order to establish a consistent incremental set of damage, strain energy release rate and stress variables. Results are obtained for non-linear response of concrete under stress paths of uniaxial compression, Brazilian test, strip loading and patch loading of prisms, and comparisons to other models and experimental values indicate reasonable correlation.

The CDM idealization forming the basis of the computational model presented is described by loading and bounding surfaces in strain energy release rate space (in contrast to stress space of elastoplasticity) and uses a parameter $R_c$ that essentially characterizes the size of the bounding surface. Numerical experiments indicated that a need exists to obtain a phenomenological relationship between $R_c$ and the compressive strength of concrete $f'_c$, as the value of 0.63 suggested in [3] was found to be limiting.

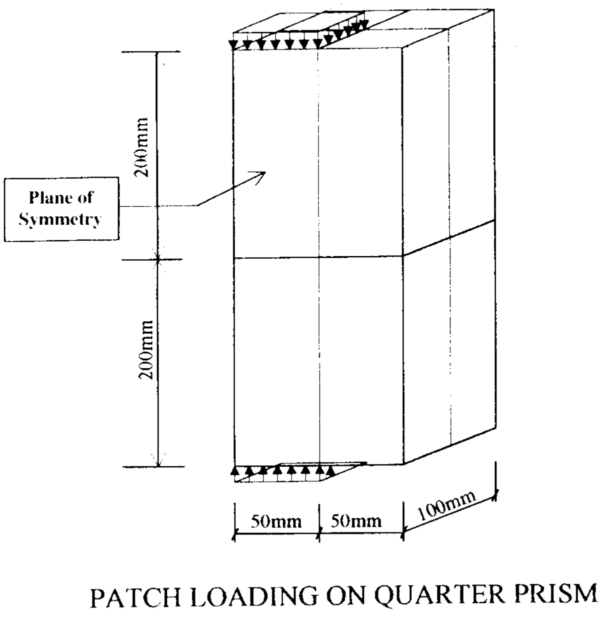


Fig. 11. Finite element mesh for concrete prism under patch loading.


## Acknowledgements

The authors are indebted to the Dept of Civil Engineering, King Fahd University of Petroleum and Minerals, for their support in the pursuit of this work.


## Appendix A

Following are the elements of the $\mathbf{D}_{\mathrm{I}}$ matrix (3 × 3):

$$\mathbf{D}_{\mathrm{I}}(1,1)=\frac{(1-\alpha\omega_1)(1-\nu^2(1-\alpha\omega_2)(1-\alpha\omega_3))}{A}E_0$$

$$\mathbf{D}_{\mathrm{I}}(1,2)=\frac{\nu(1-\alpha\omega_1)(1-\alpha\omega_2)(1+\nu(1-\alpha\omega_3))}{A}E_0$$

$$\mathbf{D}_{\mathrm{I}}(1,3)=\frac{\nu(1-\alpha\omega_1)(1-\alpha\omega_3)(1+\nu(1-\alpha\omega_2))}{A}E_0$$

$$\mathbf{D}_{\mathrm{I}}(2,1)=\frac{\nu(1-\alpha\omega_1)(1-\alpha\omega_2)(1+\nu(1-\alpha\omega_3))}{A}E_0$$

$$\mathbf{D}_{\mathrm{I}}(2,2)=\frac{(1-\alpha\omega_2)(1-\nu^2(1-\alpha\omega_1)(1-\alpha\omega_3))}{A}E_0$$

$$\mathbf{D}_{\mathrm{I}}(2,3)=\frac{\nu(1-\alpha\omega_2)(1-\alpha\omega_3)(1+\nu(1-\alpha\omega_1))}{A}E_0$$

$$\mathbf{D}_{\mathrm{I}}(3,1)=\frac{\nu(1-\alpha\omega_1)(1-\alpha\omega_3)(1+\nu(1-\alpha\omega_2))}{A}E_0$$

$$\mathbf{D}_{\mathrm{I}}(3,2)=\frac{\nu(1-\alpha\omega_2)(1-\alpha\omega_3)(1+\nu(1-\alpha\omega_1))}{A}E_0$$

$$\mathbf{D}_{\mathrm{I}}(3,3)=\frac{(1-\alpha\omega_3)(1-\nu^2(1-\alpha\omega_1)(1-\alpha\omega_2))}{A}E_0.$$

where

$$\begin{aligned}A=1&-\nu^2((1-\alpha\omega_2)(1-\alpha\omega_3)+(1-\alpha\omega_1)(1-\alpha\omega_3)\\&+(1-\alpha\omega_1)(1-\alpha\omega_2))\\&-2\nu^3(1-\alpha\omega_1)(1-\alpha\omega_2)(1-\alpha\omega_3)\end{aligned}$$

The elements of the (3 × 3) $\mathbf{D}_{\mathrm{II}}$ matrix are given by:

$$\mathbf{D}_{//}(1,1)=\frac{\genfrac{}{}{0pt}{}{(1-\boldsymbol{\omega}_1)^2(1-\beta\boldsymbol{\omega}_2)(1-\beta\boldsymbol{\omega}_3)}{((1-\boldsymbol{\omega}_2)^2(1-\boldsymbol{\omega}_3)^2-v^2(1-\beta\boldsymbol{\omega}_1)^2(1-\beta\boldsymbol{\omega}_2)(1-\beta\boldsymbol{\omega}_3))}}{B}E_0$$

$$\mathbf{D}_{//}(1,2)=\frac{\genfrac{}{}{0pt}{}{(1-\beta\boldsymbol{\omega}_1)(1-\beta\boldsymbol{\omega}_2)(1-\beta\boldsymbol{\omega}_3)^2}{(1-\boldsymbol{\omega}_1)(1-\boldsymbol{\omega}_2)(v(1-\boldsymbol{\omega}_3)^2+v^2(1-\beta\boldsymbol{\omega}_1)(1-\beta\boldsymbol{\omega}_2))}}{B}E_0$$

$$\mathbf{D}_{//}(1,3)=\frac{\genfrac{}{}{0pt}{}{(1-\beta\boldsymbol{\omega}_1)(1-\beta\boldsymbol{\omega}_3)(1-\beta\boldsymbol{\omega}_2)^2}{(1-\boldsymbol{\omega}_1)(1-\boldsymbol{\omega}_3)(v(1-\boldsymbol{\omega}_2)^2+v^2(1-\beta\boldsymbol{\omega}_1)(1-\beta\boldsymbol{\omega}_3))}}{B}E_0$$

$$\mathbf{D}_{//}(2,1)=\frac{\genfrac{}{}{0pt}{}{(1-\beta\boldsymbol{\omega}_1)(1-\beta\boldsymbol{\omega}_2)(1-\beta\boldsymbol{\omega}_3)^2}{(1-\boldsymbol{\omega}_1)(1-\boldsymbol{\omega}_2)(v(1-\boldsymbol{\omega}_3)^2+v^2(1-\beta\boldsymbol{\omega}_1)(1-\beta\boldsymbol{\omega}_2))}}{B}E_0$$

$$\mathbf{D}_{//}(2,2)=\frac{\genfrac{}{}{0pt}{}{(1-\boldsymbol{\omega}_2)^2(1-\beta\boldsymbol{\omega}_1)(1-\beta\boldsymbol{\omega}_3)}{((1-\boldsymbol{\omega}_1)^2(1-\boldsymbol{\omega}_3)^2-v^2(1-\beta\boldsymbol{\omega}_1)(1-\beta\boldsymbol{\omega}_2)^2(1-\beta\boldsymbol{\omega}_3))}}{B}E_0$$

$$\mathbf{D}_{//}(2,3)=\frac{\genfrac{}{}{0pt}{}{(1-\beta\boldsymbol{\omega}_1)^2(1-\beta\boldsymbol{\omega}_2)(1-\beta\boldsymbol{\omega}_3)^2}{(1-\boldsymbol{\omega}_2)(1-\boldsymbol{\omega}_3)(v(1-\boldsymbol{\omega}_1)^2+v^2(1-\boldsymbol{\omega}_2)(1-\beta\boldsymbol{\omega}_3))}}{B}E_0$$

$$\mathbf{D}_{//}(3,1)=\frac{\genfrac{}{}{0pt}{}{(1-\beta\boldsymbol{\omega}_1)(1-\beta\boldsymbol{\omega}_3)(1-\beta\boldsymbol{\omega}_2)^2}{(1-\boldsymbol{\omega}_1)(1-\boldsymbol{\omega}_3)(v(1-\boldsymbol{\omega}_2)^2+v^2(1-\beta\boldsymbol{\omega}_1)(1-\beta\boldsymbol{\omega}_3))}}{B}E_0$$

$$\mathbf{D}_{//}(3,2)=\frac{\genfrac{}{}{0pt}{}{(1-\beta\boldsymbol{\omega}_1)^2(1-\beta\boldsymbol{\omega}_2)(1-\beta\boldsymbol{\omega}_3)^2}{(1-\boldsymbol{\omega}_2)(1-\boldsymbol{\omega}_3)(v(1-\boldsymbol{\omega}_1)^2+v^2(1-\beta\boldsymbol{\omega}_2)(1-\beta\boldsymbol{\omega}_3))}}{B}E_0$$

$$\mathbf{D}_{//}(3,3)=\frac{\genfrac{}{}{0pt}{}{(1-\boldsymbol{\omega}_3)^2(1-\beta\boldsymbol{\omega}_1)(1-\beta\boldsymbol{\omega}_2)}{((1-\boldsymbol{\omega}_1)^2(1-\boldsymbol{\omega}_2)^2-v^2(1-\beta\boldsymbol{\omega}_1)(1-\beta\boldsymbol{\omega}_2)(1-\beta\boldsymbol{\omega}_3)^2)}}{B}E_0,$$

where

$$\begin{aligned}B=\{&(1-\boldsymbol{\omega}_1)^2(1-\boldsymbol{\omega}_2)^2(1-\boldsymbol{\omega}_3)^2\\&-v^2((1-\beta\boldsymbol{\omega}_1)(1-\beta\boldsymbol{\omega}_2)(1-\beta\boldsymbol{\omega}_3)^2\\&+(1-\beta\boldsymbol{\omega}_1)^2(1-\beta\boldsymbol{\omega}_2)(1-\beta\boldsymbol{\omega}_3)(1-\boldsymbol{\omega}_1)^2\\&+(1-\beta\boldsymbol{\omega}_1)(1-\beta\boldsymbol{\omega}_2)^2(1-\beta\boldsymbol{\omega}_3)(1-\boldsymbol{\omega}_2)^2)\\&-2v^3((1-\beta\boldsymbol{\omega}_1)^2(1-\beta\boldsymbol{\omega}_2)^2(1-\beta\boldsymbol{\omega}_3)^2)\}\end{aligned}$$

## References

[1] Krajcinovic D, Fonseka U. The continuous damage theory for brittle materials. J Appl Mech 1981;48(4):809–24.

[2] Mazars J, Pijaudier-Cabot G. Continuum damage theory—application to concrete. J Engng Mech, American Society of Civil Engineers 1989;115(2):345–65.

[3] Suaris W, Ouyang C, Fernando VM. Damage model for cyclic loading of concrete. J Engng Mech, American Society of Civil Engineers 1990;116(5):1020–35.

[4] Lee H, Pery K, Wang J. An anisotropic damage criterion for deformation instability and its application to forming limit analysis of metal plates. Engng Fracture Mech 1985;21(5):1031–54.

[5] Chow CL, Wang J. A finite element analysis of continuum damage mechanics for ductile fracture. Int J Fracture 1988;38:89–102.

[6] Chow CL, Wang J. Crack propagation in mixed-mode ductile fracture with continuum damage mechanics. Proc Inst Mech Engrs 1989;203:189–99.

[7] Ghrib F, Tinawi R. Nonlinear behavior of concrete dams using damage mechanics. J Engng Mech, American Society of Civil Engineers 1995;121(4):513–27.

[8] Dafalias YF, Popov EP. Cyclic loading for materials with a vanishing elastic region. Nuclear Engng Design 1977;41:293–302.

[9] Khan AR, Al-Gadhib AH, Baluch MH. An elasto-damage constitutive model for high strength concrete. In: Proceedings of the EURO-C 1998 Conference on Computational Modelling of Concrete Structures, Badgastein, Austria. 1998;1:133–42.

[10] Hinton E, Owen DRJ. An introduction to finite element computations. London: Pineridge Press, 1979.

[11] Hinton E, Owen DRJ. Finite elements in plasticity, theory and practice. Swansea, U.K.: Pineridge Press, 1980.

[12] Resende L. A damage mechanics constitutive theory for the inelastic behavior of concrete. Computational Methods in Appl Mech Engng 1987;60:57–93.

[13] Gonzales VF, Kotsovos MD, Pavlovic MN. Nonlinear finite element analysis of concrete structures: performance of a three-dimensional brittle model. Computers & Structures 1991;40(5):1287–306.

[14] Niyogi SK. Concrete bearing strength—support, mix, size effect. J Struct Div, American Society of Civil Engineers 1974;:1685–702.